International Journal of Fatigue 162 (2022) 106971

Contents lists available at ScienceDirect

International Journal of Fatigue

journal homepage: www.elsevier.com/locate/ijfatigue

The effect of dwell times and minimum temperature on out-of-phase thermomechanical fatigue crack propagation in a steam turbine steel—Crack closure prediction

Ahmed Azeez [a,*], Robert Eriksson [a], Viktor Norman [b], Daniel Leidermark [a], Johan Moverare [b]

[a] Division of Solid Mechanics, Department of Management and Engineering, Linköping University, SE-581 83 Linköping, Sweden
[b] Division of Engineering Materials, Department of Management and Engineering, Linköping University, SE-581 83 Linköping, Sweden

ARTICLE INFO

Keywords:
Thermomechanical fatigue
Fatigue crack growth
High temperature steel
Crack closure
Numerical modelling

ABSTRACT

Exploring crack growth behaviour is needed to establish accurate fatigue life predictions. Cracked specimens were tested under strain-controlled out-of-phase thermomechanical fatigue conditions. The tests included dwell times and three different minimum temperatures. Higher minimum temperature gave faster crack growth rates while the additions of dwell times showed no effects. Crack closure was observed in all the tests where the addition of dwell times and change in minimum temperature displayed little to no effect on crack closure stresses. Finite element models with a sharp stationary crack and material parameters switching provided acceptable predictions for the maximum, minimum, and crack closure stresses.

1. Introduction

Shifting conventional turbines towards flexible operation enables them to support renewable energy systems. As renewable energy sources have an intermittent nature, flexible operations of turbines are necessary to satisfy the energy stability and quickly fulfil the energy demands [1,2]. However, enabling flexible operation of a steam turbine results in frequent and fast start-ups, which could negatively impact the turbine components life span [3,4]. For thick-walled components subjected to high-temperature, such as the high-pressure and the intermediate-pressure steam turbine casing, large temperature gradients during fast start-ups create high thermal stresses in the component [4,5]. In turn, this leads to localised irreversible damage that, with frequent turbine operation, eventually may lead to the initiation and growth of cracks.

The loading cycle for such high-temperature components includes a simultaneous change in both temperature and load, i.e. thermomechanical fatigue (TMF) loading condition [6]. To determine the life of the turbine components with accuracy under TMF loading, a life prediction model that is less conservative must be established. This can be achieved by allowing the turbine components to operate past the crack initiation phase and within a safe limit of the crack propagation phase. Thus, investigating and understanding crack growth behaviour is essential in providing fatigue life prediction models that increase the life of the turbine components. This understanding would also allow for the assessment of the remaining life when a major crack is discovered during turbine operations.

Experimental testing using a TMF loading cycle is preferable as it provides conditions closer to the component compared to isothermal testing. Investigating the TMF life behaviour using smooth specimens has been widely employed, for which testing standardisation has already been well documented [7]. However, crack propagation behaviour has been mainly investigated under isothermal testing due to the complexity of TMF crack propagation testing. Thus, to achieve accurate life predictions models within the crack growth phase, TMF crack propagation testing is needed. Several studies have been carried out to increase the knowledge and establish guidelines related to TMF crack growth testing [8–11]. The type of the TMF loading cycle used in testing generally depends on the target component being investigated. In the current study, an out-of-phase (OP) TMF cycle was utilised to approximate the loading behaviour of the high-temperature inner casing of a steam turbine.

Researchers have carried out TMF crack propagation testing to explore and model the crack growth behaviour of different materials. For nickel-based polycrystalline alloys, both in-phase (IP) and OP types of TMF crack growth have been investigated, and faster crack growth rates were observed for IP-TMF tests compared to the OP-TMF tests [12]. Furthermore, several IP- and OP-TMF crack propagation tests showed load ratio dependency due to crack closure [8,13–15]. The use of an effective stress intensity factor [16] was shown to be successful

* Corresponding author.
E-mail address: ahmed.azeez@liu.se (A. Azeez).

https://doi.org/10.1016/j.ijfatigue.2022.106971
Received 10 December 2021; Received in revised form 15 March 2022; Accepted 29 April 2022
Available online 7 May 2022

in compensating for the crack closure behaviour where TMF crack growth curves with different load ratios collapsed together [14,15]. Other researchers were able to utilise the effective J-integral range in compensating for the load ratio effects [8,13]. In general, crack growth rates were seen to be higher for OP-TMF tests compared to isothermal tests carried out at temperatures similar to the minimum temperature of the OP-TMF tests [12,14]. However, after compensating for the load ratio dependency seen in these TMF tests, the crack growth rates of both the TMF and the isothermal tests coincided [14,15]. Crack propagation tests performed on titanium alloys showed similar behaviour where crack growth rates of OP-TMF tests coincided with isothermal tests [17]. For high-temperature steam turbine steel, accounting for the crack closure observed in OP-TMF tests was also seen to collapse the crack growth curves on an isothermal test [18]. Investigation on heat resistance steels under thermo-mechanical fatigue conditions showed an acceleration in crack growth due to pre-ageing, where microstructural evaluation showed deterioration in both creep and fatigue strength [19]. Crack growth testing performed on 12% Cr ferritic/martensitic steel showed an increase in crack growth rates with the decrease in frequency, while longer dwell times led to larger crack growth rates even at a low temperature of 300 °C [20]. For ferritic steels used in high-temperature applications, higher crack growth rates have been observed with the increase in temperature [21,22]. Additionally, the crack growth rates following Paris law showed similar exponent value for tests performed at 600 °C and below [22]. For single-crystal nickel-based alloys, the OP-TMF crack propagation tests were seen to be insensitive to the change in the maximum temperature and the dwell time of the cycle [23]. In addition, isothermal tests performed at the minimum temperature of the OP-TMF tests showed lower crack growth rates. This was likely due to the difference in the thermal exposure where microstructural investigations showed a difference between the OP-TMF and the isothermal tests [23]. Isothermal crack propagation testing on nickel-based polycrystalline alloys showed that the increase in temperature, the addition of dwell times at the maximum load, and the increase in dwell time duration would all increase the crack growth rates [24].

For testing performed on smooth specimens made of nickel-based alloys, the fatigue life of OP-TMF tests was shorter than the isothermal tests performed at the same minimum temperature of the OP-TMF cycle [25,26]. In nickel-based polycrystalline alloy, both the OP-TMF and the isothermal tests showed similar fracture dominated mode, i.e. transgranular fracture [26]. In single-crystal nickel-based alloy, the reduction of fatigue life in OP-TMF was explained by the increase in initiation and growth of surface cracks compared to the isothermal test [25]. In 9–12% Cr steels, the fatigue life under OP-TMF conditions was observed to be worst compared to IP-TMF and isothermal tests where the maximum tensile stresses are thought to have a strong influence on the fatigue life [27,28]. The addition of dwell time at the maximum stress of IP-TMF tests was observed to cause a significant reduction in fatigue life due to the acceleration of oxide scaling and microstructure evolution [28]. Furthermore, cyclic softening behaviour has been commonly observed for 9–12% Cr steels, which become more pronounced under creep-fatigue conditions [29–31].

Crack closure behaviour in which the crack is only fully open during part of the fatigue cycle is known to influence the crack growth behaviour. Contributions from the compressive part of the fatigue cycle, i.e. due to the crack not being closed, has been seen to contribute to the crack growth behaviour [32]. Identifying the crack closure stress level is essential in compensating for its effects where the crack opening stress, i.e. the stress at which the crack is fully open during loading, is commonly used. Nevertheless, the crack closing stress, i.e. the stress at which the crack just started to close during unloading, can also be used and was seen to be lower than the opening stress [18,33]. Numerical predictions of closure stress have been used where 2D and 3D finite element (FE) models can be utilised [15,34,35]. A strip yield model has been seen to predict the crack opening stress for IP- and OP-TMF tests [36]. Other techniques, including digital image correlation, has also been used to identify the crack closure levels [37]. Another study showed that the residual stresses introduced by the inelastic deformation in the initial cycle of the crack propagation test could be used to compensate for the load ratio dependency [38].

Within this work, OP-TMF crack propagation testing was performed in strain control conditions on high-temperature steam turbine steel known as FB2. The OP-TMF testing included dwell times and three different minimum temperatures to investigate their effects on the crack growth behaviour, which was not included in the previous work by Azeez et al. [18]. Crack closure was estimated using both experimental results and predicted from FE simulations. The previous work by Azeez et al. [18] used a global approach following a compliance method to obtain the crack closure stresses. In the current work, a local approach referred to as the crack surface contact area method is introduced to predict the closure stresses from the FE simulated cycles based on the FE contact area of the sharp crack. Within this study, an improved three-dimensional FE model is utilised, which reduces the limitations of the original model introduced in the previous work by Azeez et al. [18]. The improvements include accounting for the cyclic softening behaviour of the investigated material, FB2 steel, which was observed in Ref. [39]. The improved FE model included the addition of dwell times and aimed to provide better approximations for the maximum stress, minimum stress and crack closure stresses of the OP-TMF cycle.

2. Material and testing

2.1. Material

A steam turbine steel FB2 (9Cr-1Mo-1Co-0.2V-0.07Nb-0.01B-0.02N, all in wt%) was used in all the testing done within this study. The FB2 steel was the outcome of the European development of 9–12% Cr steel class under the program of Cooperation in Science and Technology (COST) 522 (1998–2003) [40–43]. The 9–12% Cr steels are widely known for their high creep strength and steam oxidation resistance which make them favourable for use at high-temperature components of steam turbines [43–48]. The ability of FB2 steel to withstand high steam temperatures of up to about 620 °C allowed it to be utilised in state-of-the-art steam turbines with ultra-supercritical steam conditions [41–43,45,46]. The heat treatment of the FB2 steel was austenitisation and rapid cooling at 1100 °C proceeded by double stage of tempering at 570 °C and 720 °C [41]. The FB2 steel is tempered martensite which was confirmed in the microstructure investigation by Azeez et al. [39] that was carried out on the same batch of FB2 steel used in this study. The FB2 material is typically used for making forged components in the steam turbine, such as the rotor [45,46]. However, in this study, TMF conditions from steam turbine casing, a cast component, are being investigated. This is done to reduce the difficulties associated with testing coarse grain alloys.

2.2. Isothermal fatigue crack propagation

A compact tension (CT) specimen shown in Fig. 1 was used for the isothermal crack propagation testing. A schematic view of the specimen is shown in Fig. 1(a), where W is the effective width, B is the thickness, and a is the manufactured crack starter length. The detailed drawing of the specimen is presented in Fig. 1(b) with $W = 25$ mm, $B = 12.5$ mm, and $a = 11$ mm. An isothermal crack propagation test was performed at 400 °C with a load range of 3500 N and load ratio of $R = F_{min}/F_{max} = 0.05$, where F_{min} is the minimum load and F_{max} is the maximum load during the cycle. The waveform used was trapezoidal with a ramp-up of 10 s and hold of 1 s at F_{max} followed by a ramp-down of 10 s and hold of 1 s at F_{min}. Pre-cracking of the specimen was done at room temperature to establish an initial crack length of approximately

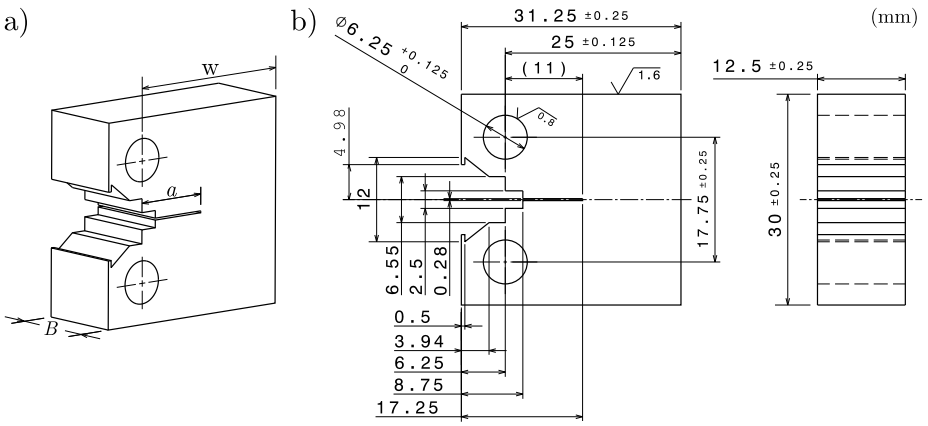

Fig. 1. Drawing of the compact tension, CT, specimen tested under isothermal fatigue crack propagation: (a) view showing the parameters W, B, and a; (b) detailed dimensions of the specimen [18].

a = 12.5 mm. After pre-cracking, the actual crack propagation test at the high temperature was performed. The outer dimensions of the CT specimen were machined, and the holes were drilled while the detailed profile was made using electrical discharge machining (EDM). No other surface finishing processes were applied.

Fig. 2 shows the testing rig, which includes a 100 kN Alwetron electromechanical test frame connected to external digital control, 580 V Doli, and a 3-zone split furnace. A pulsed direct-current potential drop system from Matelect with a currency of 5 A and frequency pulse of 1 Hz was used to measure the crack length, a, during the testing. The conversion of voltage to a for the CT specimen was carried out following a standard procedure described in Ref. [49]. The crack growth behaviour was evaluated following linear elastic fracture mechanics (LEFM), where the stress intensity factor, K, was utilised. The formulation of K can be found in several handbooks and standards, e.g. Ref. [50], as

$$K = \frac{F}{B\sqrt{W}} f_{\mathrm{CT}}\left(\frac{a}{W}\right) \tag{1}$$

where B and W are the thickness and the effective width of the specimen (see Fig. 1) while F is the applied load and f_{CT} is the geometrical factor for the CT specimen given as

$$f_{\mathrm{CT}}\left(\frac{a}{W}\right) = \frac{\left(2+\frac{a}{W}\right)}{\left(1-\frac{a}{W}\right)^{3/2}}\left(0.886 + 4.64\left(\frac{a}{W}\right) - 13.32\left(\frac{a}{W}\right)^2 + 14.72\left(\frac{a}{W}\right)^3 - 5.6\left(\frac{a}{W}\right)^4\right) \tag{2}$$

where a is the crack length (see Fig. 1). The isothermal crack propagation test evaluated in this work used the same material batch of FB2 steel, same dimension of CT specimen, and followed the same testing procedure as presented in the previous work by the authors [18].

2.3. Thermomechanical fatigue crack propagation

Cracked specimens subjected to a TMF loading cycle were used in this work to study the crack propagation behaviour. In a TMF loading cycle, both temperature and load vary with time which produces conditions closer to the actual component in focus compared to an isothermal loading cycle. An OP type of TMF cycle was chosen as it is relevant for the investigated inner casing found in the high-temperature section of steam turbines. Fig. 3 shows a schematic view of a single OP-TMF cycle where the load is seen to increase during temperature drop and vice versa. In addition, the OP-TMF cycle shows the dwell regions included at the minimum temperature, T_{min} (where the maximum load occur) and at maximum temperature, T_{max} (where the minimum load occur). Including dwell time in the TMF cycle provides a better approximation

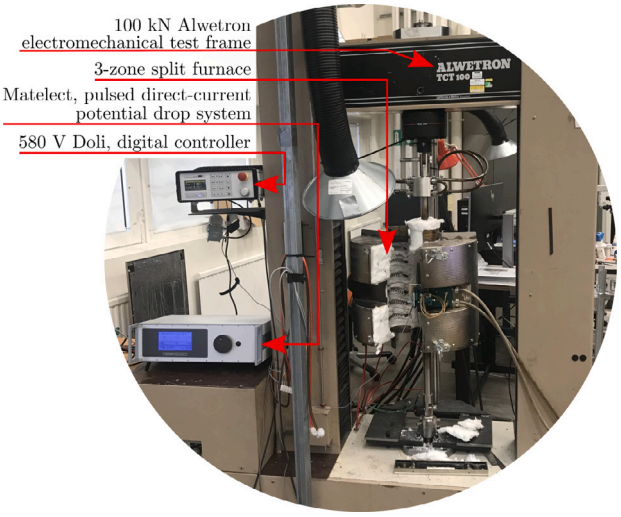

Fig. 2. The 100 kN Alwetron electromechanical test rig used for isothermal fatigue crack propagation testing.

to the loading conditions of the investigated component. The dwell at T_{max} can be thought of as the steady-state operation of the steam turbine, while the dwell at T_{min} is the shut-down. In this work, for all the OP-TMF tests, the loading curve is defined as the load that opens the crack while the unloading curve is defined as the load that closes the crack, see Fig. 3.

The OP-TMF crack propagation tests performed in this work are presented in Table 1. All the tests were strain controlled with a strain ratio of $R_\varepsilon = \varepsilon_{\mathrm{min}}/\varepsilon_{\mathrm{max}} = -\infty$, where $\varepsilon_{\mathrm{min}}$ and $\varepsilon_{\mathrm{max}}$ are the minimum and the maximum mechanical strains during the cycle. In strain-controlled tests, the nominal mechanical strain, $\varepsilon_{\mathrm{mec}}$, is typically controlled and is found by subtracting the thermal strain, $\varepsilon_{\mathrm{th}}$, (introduced by thermal expansion) from the total strain, $\varepsilon_{\mathrm{tot}}$, (measured by the extensometer). For all the performed tests, the same maximum temperature, T_{max} = 600 °C, and the same mechanical strain range, $\Delta\varepsilon_{\mathrm{mec}}$ = 0.6%, were used. Three different minimum temperature, T_{min}, of 50 °C, 100 °C, and 400 °C were investigated. Some tests included dwell time at either T_{min} or T_{max}. Dwell at T_{min} was not added for tests with $T_{\mathrm{min}} \leq 100$ °C as creep is assumed negligible at these low temperatures [39]. One of the tests, SET2-01, included a long dwell time of 24 h at T_{max} but only in the 1st cycle. This aimed at reaching stable minimum stress, σ_{min}, quickly. All the specimens were pre-crack at room temperature prior to the actual crack propagation testing. The SET2-01 test was unintentionally

Table 1
Out-of-phase thermomechanical fatigue, OP-TMF, crack growth experiments done in this work.

Specimen	T_{min}, °C	T_{max}, °C	Dwell at T_{min}	Dwell at T_{max}	Control	R_ε	$\Delta\varepsilon_{mec}$, %	l, mm
SET2–01	100	600	0 h	24 h (only 1st cycle)	Strain	−∞	0.6	2.03
SET2–02	100	600	0 min	3 min	Strain	−∞	0.6	2.03
SET2–03	400	600	0 min	3 min	Strain	−∞	0.6	2.02
SET2–04	400	600	3 min	0 min	Strain	−∞	0.6	1.96
SET2–05	400	600	0 min	0 min	Strain	−∞	0.6	2.03
SET2–06	50	600	0 min	0 min	Strain	−∞	0.6	2.08

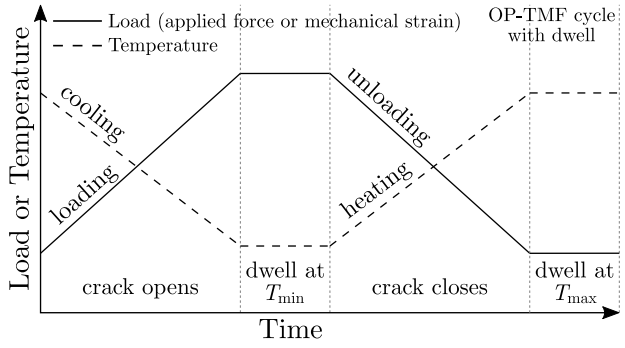

Fig. 3. A single out-of-phase thermomechanical fatigue, OP-TMF, cycle with a dwell at both the minimum temperature, T_{min}, (at the maximum load) and the maximum temperature, T_{max}, (at the minimum load).

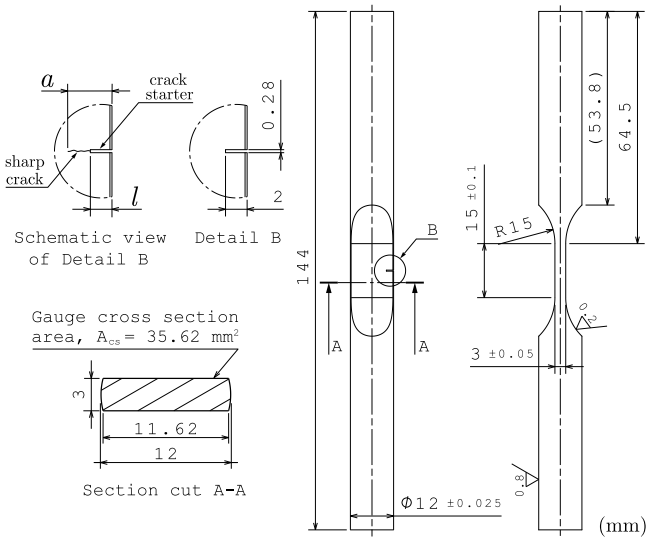

Fig. 4. The single edge crack tension, SET, specimen used for thermomechanical fatigue crack propagation testing. The measurement of the crack length, a, and the crack starter length, l, is shown in the "Schematic view of Detail B". The gauge cross-section area, A_{cs}, with no sharp crack and no crack starter is shown in the "Section cut A-A" [18].

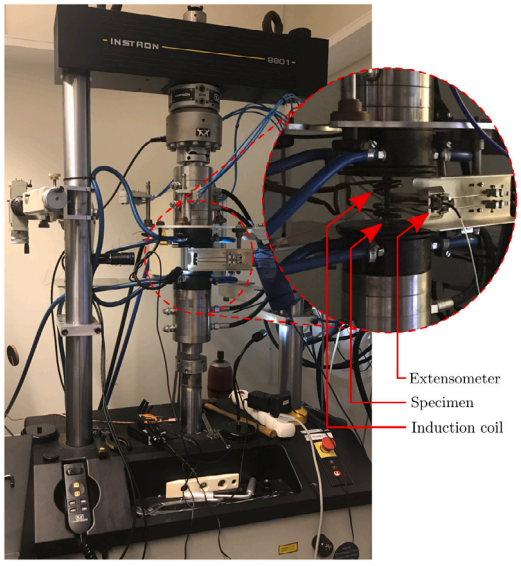

Fig. 5. Servo hydraulic testing machine, Instron 8801, used for thermomechanical fatigue crack growth testing [18].

interrupted during the 1st half cycle. The restarting process for SET2-01 was successful, and the permanent inelastic strain was compensated for. However, the data points for the 1st half cycle of SET2-01 were not recovered. The duration of the OP-TMF cycle was mainly determined by the rate of cooling and heating together with the duration of the included dwell time. A rate of 5 °C/s was generally used for both heating and cooling in all the tests. However, for SET2-06, the cooling between 100–50 °C was reduced to 1 °C/s. This allows maintaining a uniform temperature across the gauge section of the specimen during the cooling to T_{min} = 50 °C without drastically increasing the overall testing duration.

The specimens used for the OP-TMF crack propagation testing were single edge crack tension (SET) shown in Fig. 4. The specimens had a manufactured crack starter of a nominal length l of 2 mm measured from the outer edge, see "Detail B" and "Schematic view of Detail B" in Fig. 4. Turning was used to machine the specimens while both the gauge section and the manufactured crack starter were established through EDM. No other surface finishing processes were performed. After machining, the crack starter length, l, was measured for each tested specimen and reported in Table 1. The manufactured crack starter was made to aid the initiation of sharp crack during the pre-cracking process. The crack length, a, for the SET specimens was defined as the combined length of the sharp crack and the manufactured crack starter, see "Schematic view of Detail B" in Fig. 4. The area of the gauge cross-section, A_{cs} = 35.62 mm^2, can be seen in "Section cut A-A" in Fig. 4 where it is not entirely rectangular due to the curved edges.

Fig. 5 shows the testing rig, which is an Instron 8801 servo-hydraulic test machine equipped with an induction coil for heating, three compressed air nozzles for cooling, an N-type thermocouple to measure the temperature of the specimen, and an Instron extensometer 2632-055 placed over the crack starter to measure the total strain, ε_{tot}. A further detailed description of the testing rig and the testing procedure followed is described in the previous work by Azeez et al. [18].

Two compliance-based methods adapted for the change in temperature due to the TMF conditions were utilised to evaluate the OP-TMF crack propagation tests: a crack length measurement method and a crack closure stress measurement method. Both of these methods were successfully implemented and described in detail by the previous work of the authors, see Azeez et al. [18]. The crack measurement method was used to compute the crack length, a, for each cycle, N, based on the concept that a change in a would produce a change in the stiffness of the specimen. On the other hand, the crack closure stress measurement method was used to obtain the nominal stress at which the crack closure behaviour occurred. This method uses the fact that the existence of a macro-crack within the specimen would create a

change in its global stiffness depending on whether the crack faces are in contact or not. The crack closure stress measurement method was applied on the loading curve to obtain the crack opening stress, σ_{op}, and on the unloading curve, to obtain the crack closing stress, σ_{cl}, of each OP-TMF cycle (see Fig. 3) [18].

The crack growth evaluation followed LEFM and the use of stress intensity factor, K, which has the general form as

$$K = \sigma_{nom}\sqrt{\pi a} f_{SET}\left(\frac{a}{W}\right) \tag{3}$$

where σ_{nom} is the nominal stress during the cycle obtained from

$$\sigma_{nom} = \frac{F}{A_{cs}} \tag{4}$$

where F is the applied force and A_{cs} is the gauge cross-section area of the SET specimen (see "Section cut A-A" in Fig. 4). The function f_{SET} is the geometrical factor for the SET specimen given as [18]

$$\begin{aligned} f_{SET}\left(\frac{a}{W}\right) = {} & 261.22\left(\frac{a}{W}\right)^7 - 772.7\left(\frac{a}{W}\right)^6 + 918.2\left(\frac{a}{W}\right)^5 \\ & - 556.4\left(\frac{a}{W}\right)^4 + 180.51\left(\frac{a}{W}\right)^3 - 28.49\left(\frac{a}{W}\right)^2 \\ & + 2.692\left(\frac{a}{W}\right) + 1.12. \end{aligned} \tag{5}$$

where $W = 12$ mm is the width of the SET specimen and a is the crack length (see Fig. 4). Detailed description for the evaluation of the geometrical factor for the SET specimen, f_{SET}, can be found in Ref. [18].

The evaluation of K was done for mode I stress intensity factor as the crack surfaces were observed to be fairly straight. Substituting the opening, closing, maximum, and minimum nominal stresses, i.e. σ_{op}, σ_{cl}, σ_{max}, and σ_{min}, respectively, in Eq. (3) produces K_{op}, K_{cl}, K_{max}, and K_{min}, respectively, for each cycle where the crack length, a, is known.

To characterise the fatigue crack growth behaviour, the Paris power law relation was used [51]

$$\frac{da}{dN} = C\Delta K^m \tag{6}$$

where C and m are material fitting parameters while da/dN and ΔK are the crack growth rate and the stress intensity range, respectively.

The definition of ΔK usually excludes the compressive part of the fatigue cycle [52]

$$\Delta K = \begin{cases} K_{max} - K_{min} & \text{if } K_{min} > 0 \\ K_{max} & \text{if } K_{min} \le 0 \\ 0 & \text{if } K_{max} \le 0 \end{cases} \tag{7}$$

Another definition can be obtained by including the full range of the stress in the cycle producing ΔK_{fr}, i.e. the full stress intensity range,

$$\Delta K_{fr} = K_{max} - K_{min}. \tag{8}$$

Further definitions exist to account for the crack closure behaviour [16]. This is done by eliminating the part of the cycle where the crack is considered closed. For the loading part of the cycle where the crack is closed below σ_{op}, the effective opening stress intensity range, $\Delta K_{eff,op}$, can be defined as

$$\Delta K_{eff,op} = K_{max} - K_{op} \tag{9}$$

while for the unloading part of the cycle where the crack is closed below σ_{cl}, the effective closing stress intensity range, $\Delta K_{eff,op}$, can be defined as

$$\Delta K_{eff,cl} = K_{max} - K_{cl}. \tag{10}$$

3. Experimental results

All the OP-TMF crack propagation tests were performed under strain-controlled conditions with fully negative mechanical strain, ε_{mec}. Therefore, the driving force for the crack propagation comes primarily from the tensile stresses generated due to the excessive inelastic behaviour observed in the 1st cycle of all the OP-TMF tests. An example of $\sigma_{nom} - \varepsilon_{mec}$ curve of the 1st cycle from SET2-03 test (400–600 °C OP-TMF, $\Delta\varepsilon_{mec} = 0.6\%$, 3 min dwell at T_{max}) is shown in Fig. 6(a). The positive σ_{nom} in the 1st cycle is achieved as ε_{mec} goes to zero after undergoing large plasticity and creep in the 1st half-cycle as well as large stress relaxation for the tests with dwell at T_{max}. The OP-TMF tests with dwell at T_{max} in every cycle, i.e. SET2-02 and SET2-03, showed limited stress relaxation within the dwell region in the subsequent cycles in comparison to the 1st cycle, e.g. see Fig. 6(a). Some inelastic deformation can be observed even after the 1st OP-TMF cycle (see Fig. 11(a)). However, the inelastic deformation was seen to reduce with cycles and became limited after the first few hundred cycles.

Signs of crack closure was observed in all the OP-TMF tests as a visible change in the stiffness of the $\sigma_{nom} - \varepsilon_{mec}$ curves below the zero nominal stress in all cycles, e.g. see Fig. 6(a). The crack opening is defined when the change in the stiffness occurs during the loading and cooling part of the cycle, while the crack closing is defined when the change in the stiffness occurs during the unloading and heating, see Fig. 6(a) and Fig. 3. Using the crack closure stress measurement method [18], the crack opening stress and the crack closing stress (σ_{op} and σ_{cl}), i.e. the nominal stress at which the crack closure occur during the loading and the unloading, respectively, were determined for each cycle, e.g. see Fig. 6(b). The determination of σ_{op} and σ_{cl} was necessary to account for the closure effects when examining the crack propagation behaviour. It was seen that σ_{op} and σ_{cl} were not equal, and their largest difference was at the beginning of the tests when the crack length, a, was short. On the other hand, no signs of crack closure were observed in the isothermal fatigue crack propagation test performed at 400 °C as there was no change in the global stiffness seen in any of the cycles.

The minimum stress, σ_{min}, over cycles, N, for all the OP-TMF tests with minimum temperature, T_{min}, of 50 °C, 100 °C, and 400 °C are shown in Fig. 7(a), (b), and (c), respectively. All the OP-TMF tests seem to follow a linear relation between σ_{min} and N after the 1st cycle when plotted using a base-10 logarithmic scale on N. The slopes of each linear relation were observed to be similar among the different OP-TMF tests except for SET2-01 (100–600 °C OP-TMF, 24 h dwell T_{max} only at 1st cycle). For OP-TMF tests without any dwell, i.e. SET2-06 and SET2-04, a noticeable difference in σ_{min} over all the cycles was observed when using different T_{min}, see Fig. 7(a) and (c). Higher σ_{min} can be seen for SET2-06 (50–600 °C OP-TMF, no dwell) compare to SET2-04 (400–600 °C OP-TMF, no dwell). However, the dwell time of 3 min added at T_{max} for every cycle in tests SET2-2 (100–600 °C OP-TMF) and SET2-3 (400–600 °C OP-TMF) seems to make σ_{min} after the 1st cycle to relax to a similar level even though these two tests had different T_{min}, see Fig. 7(b) and (c). The addition of a 24 h dwell at T_{max} in the 1st cycle of SET2-01 (100–600 °C OP-TMF) put σ_{min} at a fairly stable level of around −200 MPa over the cycles, see Fig. 7(b). Similar levels of σ_{min} were observed between SET2-04 (400–600 °C OP-TMF, 3 min dwell at T_{min}) and SET2-05 (400–600 °C OP-TMF, no dwell) even though the test SET2-04 had dwell time of 3 min added at T_{min} in every cycle.

Furthermore, in Fig. 7(b), the long dwell of 24 h in the 1st cycle for SET2-01 put σ_{min} in the 2nd cycle at about −208 MPa, while the short dwell of 3 min in the 1st cycle for SET2-02 put σ_{min} in the 2nd cycle at about −239 MPa. Even though the dwell duration difference in the 1st cycle was huge, the difference in σ_{min} on the 2nd cycle was not that large, about 31 MPa. In addition, by observing σ_{min} in the 1st cycle for all the tests (Fig. 7), a slight dependency on the choice of T_{min} can be noticed where σ_{min} seems to decrease with the increase of T_{min}.

The maximum stress, σ_{max}, over crack length, a, for all the OP-TMF tests are shown in Fig. 8. A clear dependency can be observed between σ_{max} and a for all the OP-TMF tests, where σ_{max} drops with the increase in a. Tests with T_{min} of 50 °C and 100 °C, i.e. SET2-01, SET2-02, and SET2-06, seem to coincide. However, tests with a T_{min} of 400 °C, i.e. SET2-03, SET2-04, and SET2-05, seem to have more scatter between them and have lower σ_{max} than the other tests. This

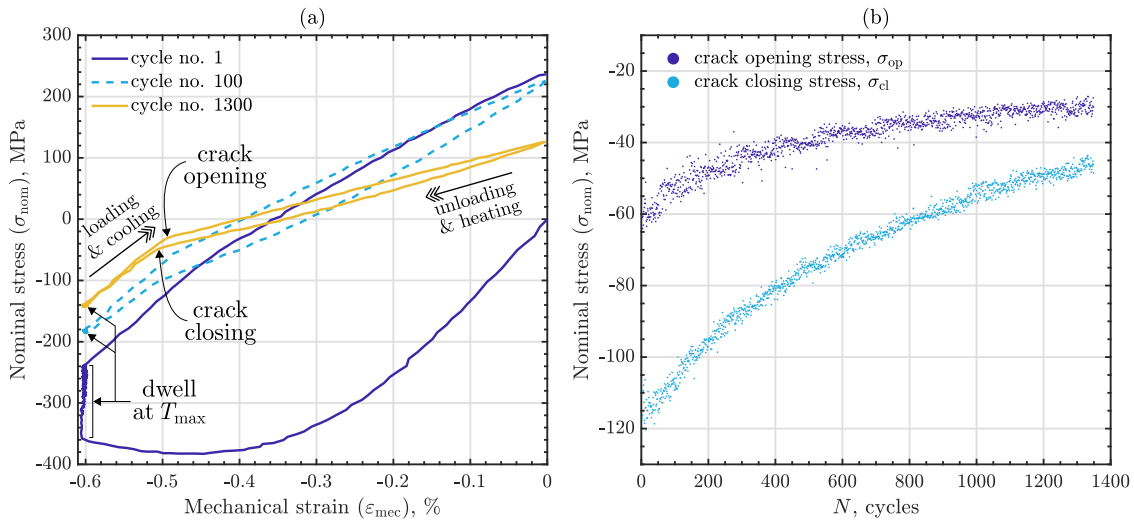

Fig. 6. Specimen SET2-03 (400–600 °C OP-TMF, 3 min dwell T_{max}) showing (a) the experimental curves, $\sigma_{nom} - \varepsilon_{mec}$, for cycles 1, 100, 1300; (b) the crack opening and closing stresses, σ_{op} and σ_{cl}, over the test cycles, N.

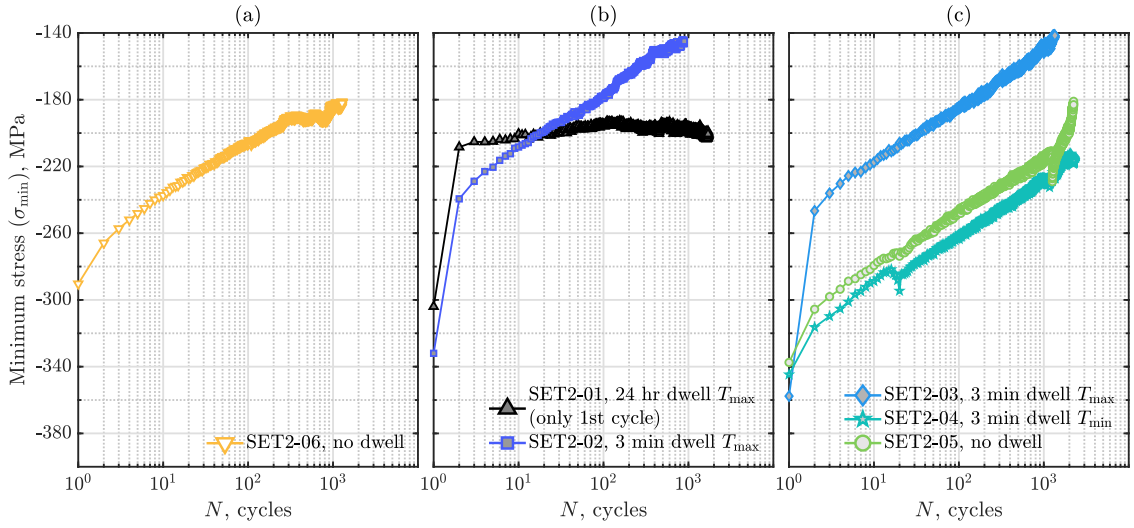

Fig. 7. Minimum stress, σ_{min}, of the out-of-phase thermomechanical fatigue crack propagation cycle versus the number of cycles, N, for the experimental tests with the minimum temperature, T_{min}, of (a) 50 °C; (b) 100 °C; and (c) 400 °C.

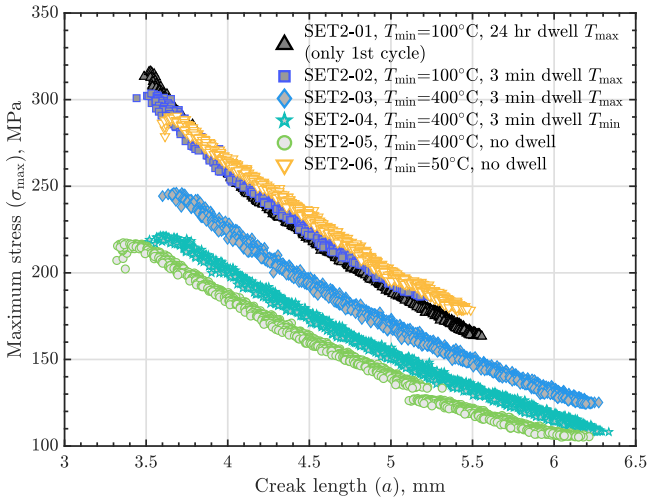

Fig. 8. Maximum stress, σ_{max}, of the out-of-phase thermomechanical fatigue crack propagation cycle over the crack length, a.

could indicate some dependency of σ_{max} on T_{min} when using high T_{min}, e.g. 400 °C.

The crack growth rate, da/dN, over ΔK, i.e. the stress intensity range excluding the compressive part of the fatigue cycle (defined in Eq. (7)), is shown in Fig. 9(a). All the OP-TMF tests can be seen to give faster crack growth rates than the isothermal crack propagation tests performed at 400 °C and 100 °C. The isothermal crack propagation test at 100 °C was taken from the previous work by the authors [18]. A dependency of the OP-TMF crack growth behaviour on T_{min} can be observed in Fig. 9(a), where faster crack growth rates can be seen for OP-TMF tests with T_{min} = 400 °C compared to the other OP-TMF tests. However, this dependency seems to vanish completely for OP-TMF tests with $T_{min} \leq 100$ °C, i.e. crack growth behaviour of SET2-06 (50–600 °C OP-TMF, no dwell) coincide with SET2-01 (100–600 °C OP-TMF, 24 h dwell at T_{max} only 1st cycle) and SET2-02 (100–600 °C OP-TMF, 3 min dwell at T_{max}). Furthermore, the use of ΔK_{fr} (defined in Eq. (8)) shown in Fig. 9(b) does not seem to provide a better prediction of the crack growth behaviour.

The crack closure behaviour observed in all the OP-TMF tests was accounted for using the effective opening stress intensity range, $\Delta K_{eff,op}$ (see Eq. (9)), and the effective closing stress intensity range, $\Delta K_{eff,cl}$

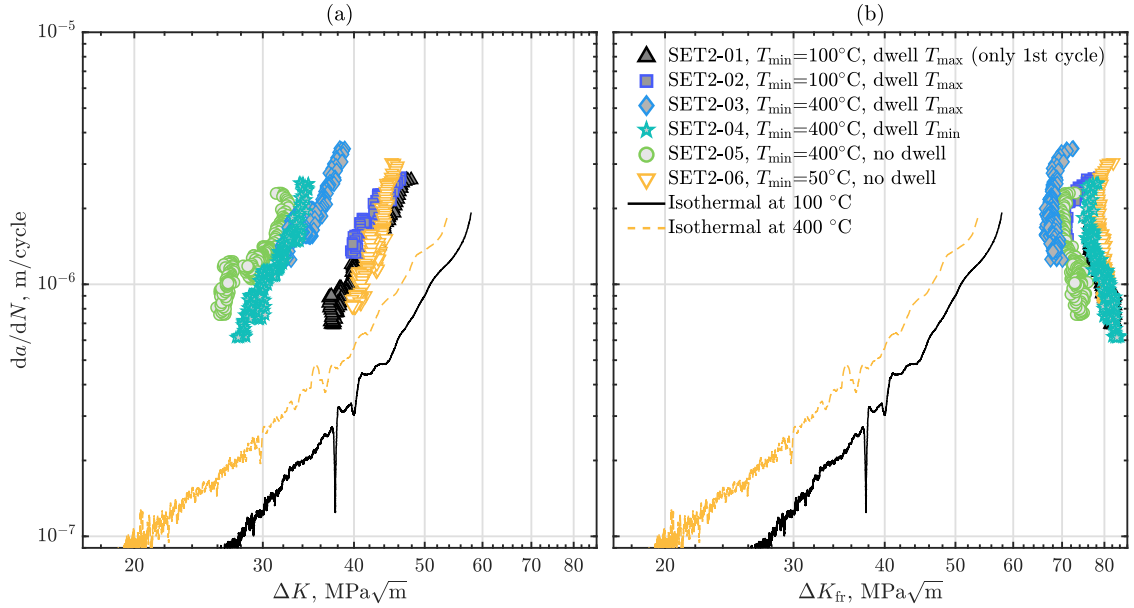

Fig. 9. Fatigue crack growth behaviour without compensating for the crack closure effects seen in all OP-TMF tests. The crack growth rate, $\mathrm{d}a/\mathrm{d}N$, is plotted versus: (a) ΔK, the stress intensity range excluding the negative part of the cycle (Eq. (7)); (b) ΔK_{fr}, the full stress intensity range (Eq. (8)).
Source: The isothermal test at 100 °C was taken from Azeez et al. [18].

(see Eq. (10)), as shown in Fig. 10(a) and (b), respectively. A collapse of the OP-TMF crack growth rates on the isothermal tests can generally be observed in both Fig. 10(a) and (b). The OP-TMF tests with $T_{\mathrm{min}} \leq 100$ °C, i.e. SET2-01, SET2-02, and SET2-06, tend to collapse over the isothermal test at 100 °C, while the OP-TMF tests with $T_{\mathrm{min}} = 400$ °C, i.e. SET2-03, SET2-04, and SET2-05, tend to collapse over the isothermal test at 400 °C. In Fig. 10(a), the use of $\Delta K_{\mathrm{eff,op}}$ to account for the crack closure measured from the loading part of the cycle shows an acceptable collapse of the OP-TMF tests with $T_{\mathrm{min}} \leq 100$ °C on the isothermal test at 100 °C. However, a weaker collapse can be observed for the OP-TMF tests with $T_{\mathrm{min}} = 400$ °C on the isothermal test at 400 °C. On the other hand, in Fig. 10(b), the use of $\Delta K_{\mathrm{eff,cl}}$ to account for closure measured from the unloading part of the cycle shows an improvement of the collapse for OP-TMF tests with $T_{\mathrm{min}} = 400$ °C on the isothermal test at 400 °C. In addition, the collapse of OP-TMF tests with $T_{\mathrm{min}} \leq 100$ °C on the isothermal test at 100 °C was also enhanced by the use of $\Delta K_{\mathrm{eff,cl}}$, see Fig. 10(b).

4. Modelling of crack closure

The crack closure behaviour observed in the OP-TMF crack propagation tests was predicted using FE simulations. The FE model used a sharp stationary crack with contact boundary conditions on the crack surfaces where no crack advancement methods or node releasing techniques were included. The FE model was originally introduced in the previous work of the authors, see Azeez et al. [18]. However, in the current work, the FE model was modified to improve the prediction of $\sigma_{\mathrm{nom}} - \varepsilon_{\mathrm{mec}}$ curves, especially for simulations with long crack length, a, where the original model showed limitations in the prediction of the minimum stress, σ_{min}. This improvement was achieved by allowing the material model to switch material parameters from initial to mid-life properties during the simulation. The material parameters switching was motivated by the cyclic softening behaviour observed from isothermal low cycle fatigue (LCF) tests performed on smooth cylindrical specimens made from the same material batch of the FB2 steel [39]. In addition, the FE model was also adapted to simulate and predict the crack closure behaviour for the OP-TMF crack propagation tests with added dwell time.

The geometry used in the FE simulations was the full SET specimen with a crack starter length of $l = 2$ mm (see Fig. 4). The SET specimen was modelled using the FE software ABAQUS [53] where the appropriate boundary conditions, loading conditions, the inclusion of a sharp crack with contact boundary conditions, and meshing were all implemented as described in Ref. [18]. All the OP-TMF tests performed in this work, i.e. the 6 tests shown in Table 1, were simulated. For each test, 7 models were built each with different crack length, a, i.e. 3.15 mm, 3.5 mm, 4.0 mm, 4.5 mm, 5.0 mm, 5.5 mm, and 6 mm.

4.1. Material model and material parameters switching

The material model used for the FE simulations consisted of cyclic elasto-plastic and creep models. The model was provided as built-in functions by the used FE software, ABAQUS [53]. The elasto-plastic model consisted of a linear elastic model and a nonlinear kinematic hardening model with two back-stresses. The model utilised associated flow rule with von Mises yield criteria. Ziegler's kinematic law plus a recall term for each of the back-stresses, $\boldsymbol{\alpha}_m$, was used to describe the evolution law of the hardening model [53]

$$\dot{\boldsymbol{\alpha}}_m = C_m \frac{\boldsymbol{\sigma} - \boldsymbol{\alpha}}{\sigma_y} \dot{\bar{\varepsilon}}^{\mathrm{p}} - \gamma_m \boldsymbol{\alpha}_m \dot{\bar{\varepsilon}}^{\mathrm{p}} \tag{11}$$

where the total back-stress tensor is

$$\boldsymbol{\alpha} = \sum_{m=1}^{2} \boldsymbol{\alpha}_m \tag{12}$$

while C_m and γ_m are temperature-dependent material parameters with $m = 1, 2$. The parameters $\dot{\boldsymbol{\alpha}}_m$, $\boldsymbol{\sigma}$, σ_y, and $\dot{\bar{\varepsilon}}^{\mathrm{p}}$ are the rate of the back-stress tensor, the stress tensor, the yield strength, and the equivalent plastic strain rate, respectively. The creep model consisted of a Norton power law as [54]

$$\dot{\bar{\varepsilon}}^{\mathrm{c}} = A \tilde{\sigma}^{n} \tag{13}$$

where A and n are temperature-dependent material parameters while $\dot{\bar{\varepsilon}}^{\mathrm{c}}$ and $\tilde{\sigma}$ are the equivalent creep strain rate and the equivalent stress, respectively. A detailed description of the employed model is given by Azeez et al. [39]. The temperature-dependent material parameters utilised for the material model, i.e. elastic, plastic, and creep parameters, were all extracted from isothermal LCF tests that were conducted previously by the authors [39]. These isothermal LCF tests

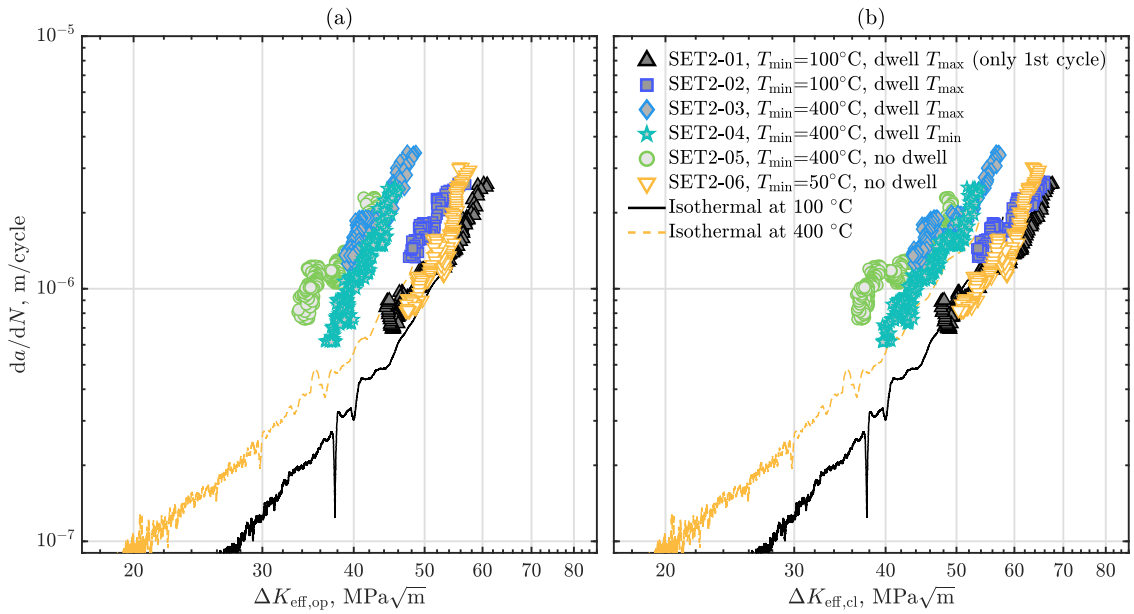

Fig. 10. Fatigue crack growth behaviour after accounting for the crack closure effects using σ_{op} and σ_{cl}. The crack growth rate, $\mathrm{d}a/\mathrm{d}N$, is plotted versus: (a) $\Delta K_{\mathrm{eff,op}}$, the effective opening stress intensity range (Eq. (9)); (b) $\Delta K_{\mathrm{eff,cl}}$, the effective closing stress intensity range (Eq. (10)).
Source: The isothermal test at 100 °C was taken from Azeez et al. [18].

Table 2
Temperature-dependent material parameters for the elasto-plastic model of the steam turbine steel FB2 for both initial and mid-life cyclic behaviour [18,39].

Cyclic behaviour	Temperature, °C	E, GPa	ν	$\Delta\varepsilon_{\mathrm{mec}}$, %	σ_y, MPa	C_1, MPa	C_2, MPa	γ_1	γ_2
Initial	20	213.97	0.285	2.0	588.40	44 680	322 985	426.07	4157.7
Initial	400	186.69	0.299	1.2	481.22	85 958	229 111	828.84	5821.7
Initial	500	179.91	0.305	1.2	420.31	101 264	257 438	870.96	5782.6
Initial	550	170.24	0.308						
Initial	600	159.41	0.312	1.2	300.20	118 360	584 880	1056.4	7054.7
Initial	625	147.36	0.314						
Mid-life	20	213.97	0.285	0.8	295.18	534 110	213 070	4509.3	648.21
Mid-life	400	186.69	0.299	0.8	226.51	125 930	389 894	502.79	4316.3
Mid-life	500	179.91	0.305	0.8	196.24	91 938	436 427	430.63	5595.9
Mid-life	550	170.24	0.308						
Mid-life	600	159.41	0.312	0.8	152.69	82 488	482 959	562.3	7006.6
Mid-life	625	147.36	0.314						

were performed on smooth cylindrical specimens made from the same material batch of the FB2 steel used in this work.

Two different sets of temperature-dependent material parameters were employed in this study. One set of the parameters represented the initial cyclic behaviour and was extracted from the initial cycles of the LCF tests. The other set of parameters represented the mid-life cyclic behaviour and were extracted from the mid-life cycles of the LCF tests with mechanical strain range, $\Delta\varepsilon_{\mathrm{mec}}$, of 0.8%. The parameters for the initial cyclic behaviour are provided in Ref. [18] while the parameters for the mid-life cyclic behaviour are provided in Ref. [39]. For both the initial and the mid-life cyclic behaviour, the elasto-plastic and creep parameters were fitted over the temperature and presented in Tables 2 and 3, respectively, where E is the elastic modulus and ν is Poisson's ratio. All the temperature-dependent material parameters for both initial and mid-life cyclic behaviour were determined and included in the FE model for every 10 °C over the temperature range 50–600 °C.

Material parameters switching is defined in this work as switching the temperature-dependent material parameters, i.e. plastic and creep parameters, during an FE simulation from the initial to the mid-life cyclic behaviour. This technique (i.e. material parameters switching) has been observed in the literature (sometimes referred to as jumping procedure) and has been successfully used by other researchers [13,55,56]. The differences between the initial and the mid-life parameters (see Tables 2 and 3) are mainly related to the cyclic softening behaviour

Table 3
Temperature-dependent material parameters for the creep model of the steam turbine steel FB2 for both initial and mid-life cyclic behaviour [18,39].

Cyclic behaviour	Temperature, °C	A, $1/(\mathrm{GPa}^n\ \mathrm{s})$	n
Initial	500	6.65×10^4	30.27
Initial	550	8.10×10^2	19.95
Initial	600	16.37	13.69
Mid-life	500	5.04×10^{13}	43.04
Mid-life	550	1.53×10^9	26.80
Mid-life	600	1.54×10^5	15.96

experienced by the material during the LCF tests. The material parameters switching is aimed at achieving better approximation for $\sigma_{\mathrm{nom}}-\varepsilon_{\mathrm{mec}}$ curves of the OP-TMF cycles. Nevertheless, using the parameters from the initial cyclic behaviour is necessary to accurately simulate the large inelastic deformation observed in the 1st half cycle of the OP-TMF tests, see Fig. 6(a) [18]. Then, shifting the parameters to the mid-life cyclic behaviour is followed, which, especially for long crack length, a, is appropriate since the actual crack propagation test has already experienced many cycles. This parameters shifting was achieved by linearly interpolating between the two sets of parameters (i.e. initial and mid-life parameters) to provide a gradual transition from the initial to the mid-life cyclic behaviour. During an FE simulation, the material parameters switching can be enabled at any desired cycle to gradually

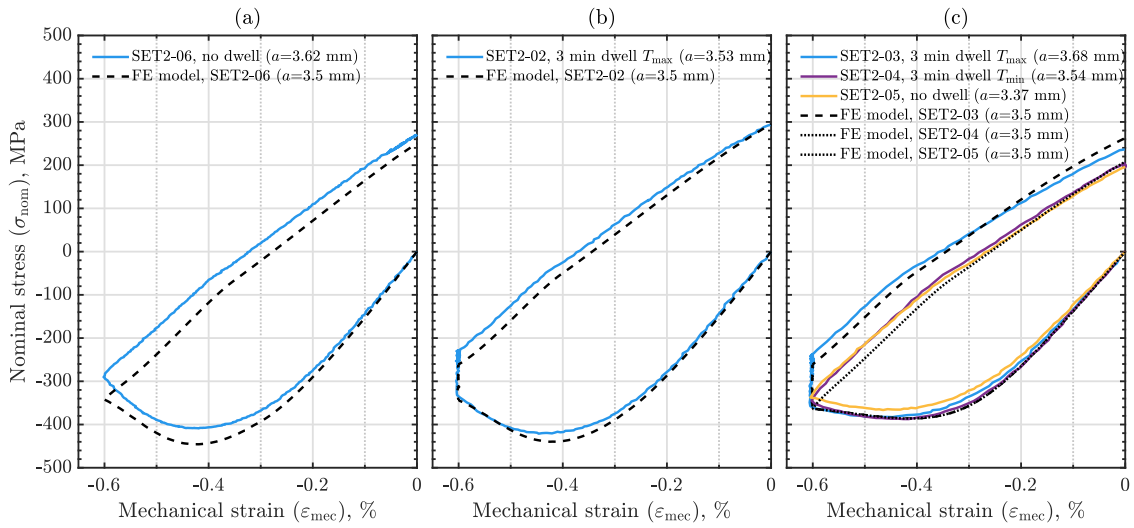

Fig. 11. Experimental and simulated $\sigma_{nom} - \varepsilon_{mec}$ curves for the 1st cycle of OP-TMF tests with known crack length, a and minimum temperature, T_{min}, of (a) 50 °C; (b) 100 °C; and (c) 400 °C.

shift from the initial to the mid-life cyclic behaviour. Convergence errors were avoided by allowing the material parameters switching to take place in the loading part of the desired cycle when simulating tests without dwell at T_{max}. However, for tests with dwell at T_{max}, the material parameter switching was done in the dwell region of the desired cycle (see Fig. 3). In all the FE simulations of the OP-TMF tests, the material parameters switching was done during the 2nd cycle except for test SET2-01 (100–600 °C OP-TMF, 24 h dwell T_{max} at 1st cycle) where it was done during the 1st cycle.

4.2. Accuracy of the finite element simulations

The FE models were constructed using sharp stationary crack, where several FE simulations were done with different crack lengths for each OP-TMF test. In all the FE simulations, the material parameters switching from initial to mid-life cyclic behaviour was generally set during the 2nd cycle. This allows the large inelastic behaviour in the 1st half-cycle of the simulations to occur as observed in the actual tests. The experimental and the simulated $\sigma_{nom} - \varepsilon_{mec}$ curves for the 1st cycles with similar crack length, a, are shown in Fig. 11(a), (b), and (c) for OP-TMF tests with T_{min} of 50 °C, 100 °C and 400 °C, respectively. Acceptable accuracy for the 1st half-cycle was observed between the experimental and the FE simulations. For the FE simulations of test SET2-01 (100–600 °C OP-TMF, 24 h dwell T_{max} at 1st cycle), the parameter switching was done during the 1st cycle since long dwell time took place at T_{max}. In addition, the long dwell was simulated for 15 min instead of the actual 24 h where the minimum stress was observed to be approximately the same due to the exponential behaviour of creep.

After switching material parameters from initial to mid-life cyclic behaviour, the simulations were run for 5 more cycles to obtain a stable cyclic behaviour. Thus, in total 7 cycles were simulated for all OP-TMF tests except for SET2-01 where 6 cycles were simulated. However, FE simulations without material parameters switching, i.e. FE simulations using parameters from the initial cyclic behaviour, were only run for 5 cycles to obtain stable cyclic behaviour. The last simulated cycles from both FE models with and without parameter switching were extracted and compared to the experimental results with the respective crack length, a. An FE model with parameter switching to mid-life behaviour provided a better approximation of $\sigma_{nom} - \varepsilon_{mec}$ curves to the experimental data. An example is shown in Fig. 12(a), (b), and (c) for test SET2-05 (400–600 °C OP-TMF without dwell) with three different a of 3.5 mm, 4.5 mm, and 5.5 mm, respectively. For long a, the simulated cycles with parameters switching to mid-life showed good approximation to the experimental cycles. For short a, the simulated cycles with parameter switching were slightly wider and had slightly higher minimum stress than the experimental cycles. However, since the FE simulations with material parameters switching showed acceptable accuracy to the experimental results, the crack closure predictions were only taken from FE models with material parameters switching.

Comparing the minimum stress, σ_{min}, of the experimental tests to the FE simulations with material parameter switching is shown in Fig. 13(a), (b), and (c) for OP-TMF tests with T_{min} of 50 °C, 100 °C, and 400 °C, respectively. Generally, an acceptable prediction of the experimental results was achieved using the FE simulations, especially for crack length of $a \geq 4$ mm. For the OP-TMF test with the 24 h dwell in the 1st cycle at T_{max}, i.e. SET2-01, the FE simulation does not seem to predict the stable behaviour of σ_{min} seen in the experimental results, see Fig. 13(b). However, as the maximum difference between the experimental and the FE results for SET2-01 was not significant, about 30 MPa, the FE prediction was considered acceptable. In the FE simulations, the addition of 3 min dwell at T_{max} provides an increase in σ_{min} similar to the experimental results, see FE model for SET2-02 and SET2-03 in Fig. 13(b) and (c). On the other hand, the addition of dwell at T_{min} does not seem to affect σ_{min} where it collapses with the FE simulations without any dwell. Furthermore, all the FE simulations with material parameters switching were observed to predict the maximum stress, σ_{max}, of the experimental results fairly well as shown in Fig. 14.

4.3. Prediction of crack closure

Change in the global stiffness below zero nominal stress was observed in all the FE modelled $\sigma_{nom} - \varepsilon_{mec}$ curves of all the simulated OP-TMF tests, e.g. see Fig. 12. This change in the stiffness indicates the presence of crack closure in these FE models, which were built using a sharp stationary crack with crack surface contacts. The last cycle of the FE simulations with material parameter switching was utilised to predict the crack closure stresses.

Through the use of the FE modelling, the FE contact area of the sharp crack, $A_{c,FE}$, was used to obtain the crack closure stresses, i.e. FE σ_{op} and FE σ_{cl}, from the simulated cycles. The contact area parameter, $A_{c,FE}$, is at its maximum value when the crack is fully closed and it is zero when the crack is fully open. The point of the crack opening is defined when $A_{c,FE}$ switches from non-zero to zero value during loading, while the point of crack closing is defined when $A_{c,FE}$ switches from zero to non-zero value during unloading, see Fig. 15(b). The

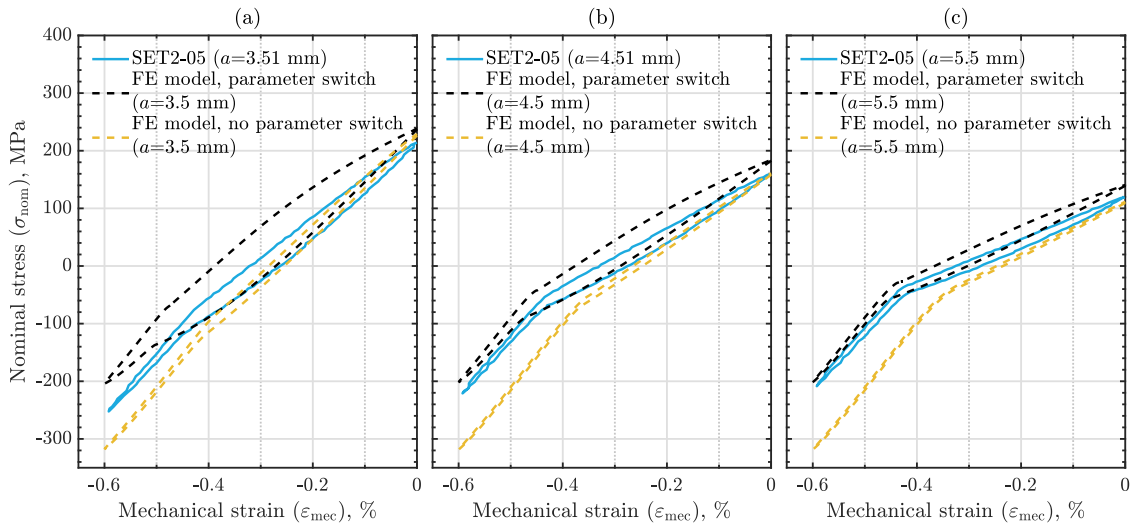

Fig. 12. Simulated $\sigma_{nom} - \varepsilon_{mec}$ curves with and without material parameter switching compared to experimental results for SET2-05 test (400–600 °C OP-TMF, no dwell) for crack lengths, a, of (a) 3.5 mm; (b) 4.5 mm; and (c) 5.5 mm.

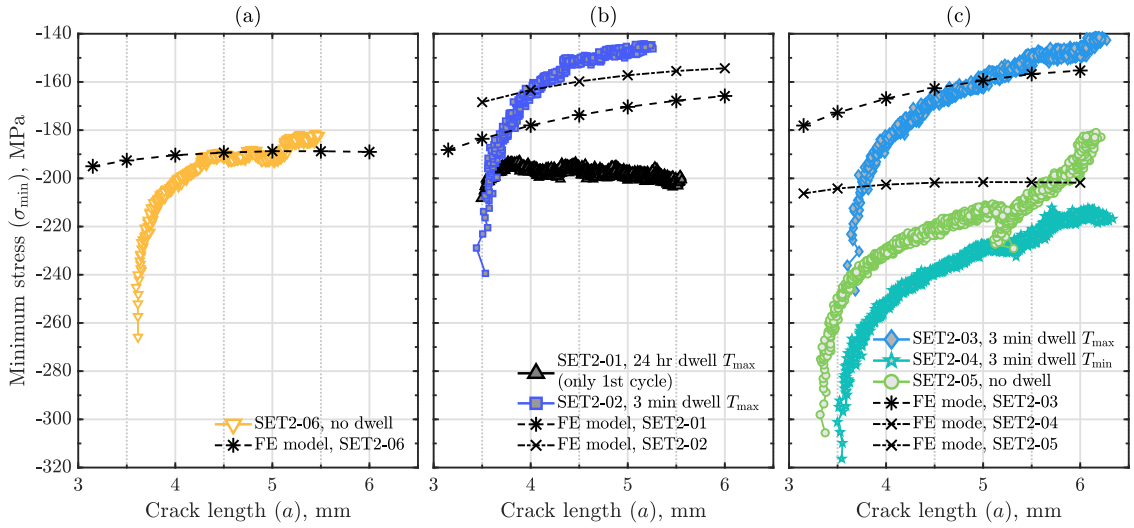

Fig. 13. Minimum stress of the cycle, σ_{min}, over the crack length, a for experimental tests and finite element simulations with material parameters switching of OP-TMF tests with minimum temperature, T_{min}, of (a) 50 °C; (b) 100 °C; and (c) 400 °C.

maximum value of $A_{c,FE}$ represent the total surface area of one side of the sharp crack, which can be computed as

$$A_{c,FE}^{max} = W(a - l) \tag{14}$$

where a is the crack length while $l = 2$ mm is the crack starter length and $W = 3$ mm is the width of the gauge section for the SET specimen, see Fig. 4. By setting a small percentage limit based on the maximum $A_{c,FE}$, it becomes possible to determine the nominal stresses at which the sharp crack is slightly closed, i.e. closed by the set percentage limit. Reaching this limit during the loading part of the cycle gives the crack opening stress, FE σ_{op}, while reaching the limit during the unloading part of the cycle gives the crack closing stress, FE σ_{cl}. In this work, the percentage limit was chosen to be 1% of $A_{c,FE}^{max}$ for a given crack length, a (see Eq. (14)).

An example of the FE modelled $\sigma_{nom} - \varepsilon_{mec}$ curves and $\sigma_{nom} - A_{c,FE}$ curves for SET2-05 (400–600 °C OP-TMF, no dwell) are shown in Fig. 15(a) and (b), respectively, with two crack lengths, a, of 3.5 mm and 6.0 mm. In Fig. 15(a), the compliance crack closure stress measurement method (used on the experimental cycles in Section 3) was applied to obtain FE $\sigma_{op,comp}$ and FE $\sigma_{cl,comp}$. In Fig. 15(b), the crack surface contact area method was applied to obtain FE σ_{op} and FE σ_{cl}. It was observed that the use of the compliance method for long crack lengths gives approximately similar results of the crack closure stresses to the crack surface contact area method. However, for short crack lengths i.e. $a \leq 4$ mm, the compliance method was seen to usually fail or predict inaccurate values of crack closing stress, FE $\sigma_{cl,comp}$, compare to the crack surface contact area method, FE σ_{cl}, see Fig. 15(a). Nevertheless, the crack opening stress does not seem to differ between the two methods (FE $\sigma_{cl,comp}$ similar to FE σ_{op}), see Fig. 15(a) and (b).

The FE contact area of the sharp crack, $A_{c,FE}$, was seen to change quickly within small range of σ_{nom} for models with long crack length, e.g. the low slope of $\sigma_{nom} - A_{c,FE}$ curve in Fig. 15(b) for $a = 6.0$ mm. However, this behaviour becomes less pronounced with a shorter crack length. It was also seen that the maximum value of $A_{c,FE}$ was never reached after the first simulated cycle, indicating that the crack in the FE simulations was never fully closed even at the minimum stress of the cycle, σ_{min}.

The crack surface contact area method was applied on the last modelled cycle, i.e. the 5th cycle after the material parameter switching, for all the FE simulation to obtain the FE crack opening and closing stresses, i.e. FE σ_{op} and FE σ_{cl}. The crack closure stresses over crack length, a, obtained from the experimental cycles as well as from the

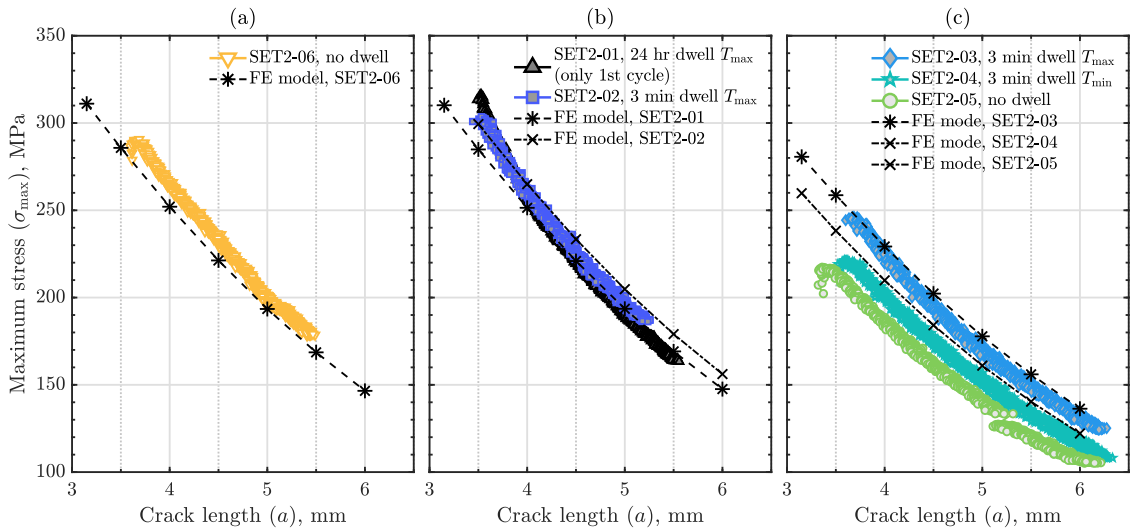

Fig. 14. Maximum stress of the cycle, σ_{max}, over the crack length, a for experimental tests and finite element simulations with material parameters switching of OP-TMF tests with minimum temperature, T_{min}, of (a) 50 °C; (b) 100 °C; and (c) 400 °C.

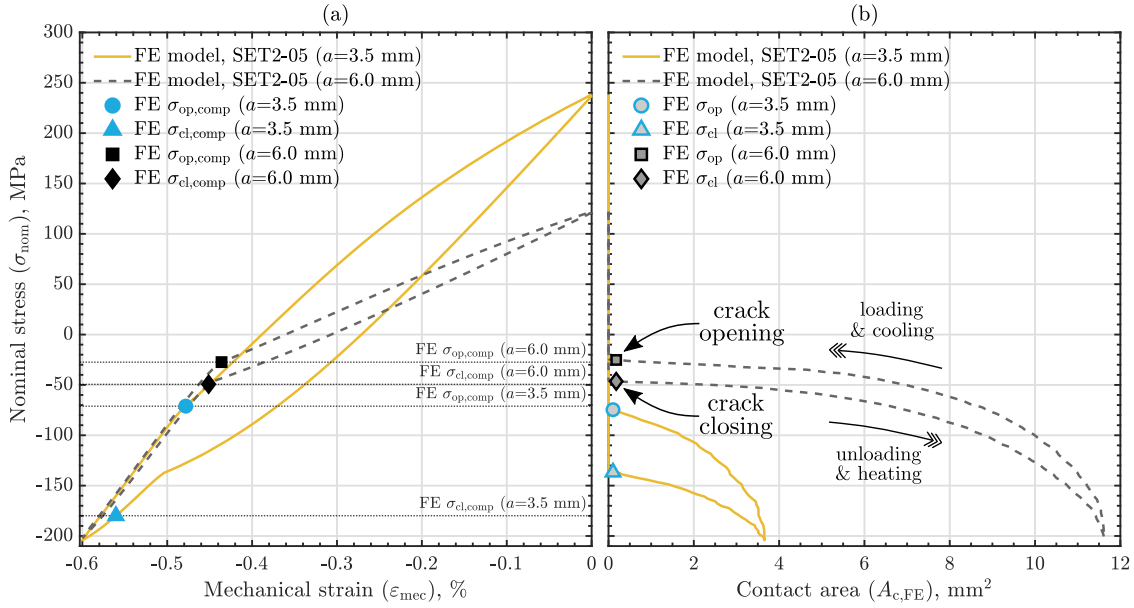

Fig. 15. FE model of SET2-05 (400–600 °C OP-TMF, no dwell) for two crack lengths, a, of 3.5 mm and 6.0 mm showing (a) $\sigma_{nom} - \varepsilon_{mec}$ curves where compliance method was used to obtain FE $\sigma_{op,comp}$ and FE $\sigma_{op,comp}$; and (b) $\sigma_{nom} - A_{c,FE}$ curves where the crack surface contact area method was used to obtain FE σ_{op} and FE σ_{op}.

FE modelled cycles for all the OP-TMF tests are shown in Fig. 16. The FE crack opening and closing stresses (FE σ_{op} and FE σ_{cl}) over a for each OP-TMF test were fitted using a 2nd degree polynomial. No clear distinction can be observed among the different OP-TMF tests for both crack opening and closing stresses using the experimental or the FE results, see Fig. 16. This indicates that the additions of long dwell in the 1st cycle and the addition of short dwell in every cycle do not have a major effect on the crack closure stresses. Also, the use of different minimum temperatures, T_{min}, (i.e. 50 °C, 100 °C and 400 °C) does not seem to produce any difference in the crack closure stresses. The FE crack opening and closing stresses obtained using the crack surface contact area method, i.e. FE σ_{op} and FE σ_{cl}, were seen to predict the experimental results fairly well for all the simulated crack lengths. In general, the crack closing stress was seen to be lower than the crack opening stress for both experimental and FE results, and their maximum difference occurred at short crack lengths. However, the difference between the opening and the closing stresses seem to reduce with the increase in crack length.

Substituting FE σ_{op} and FE σ_{cl} in Eq. (3) gives the stress intensity factors for the FE crack closure stresses, i.e. FE K_{op} and FE K_{cl}. Then, the FE effective opening and closing stress intensity ranges, i.e. FE $\Delta K_{eff,op}$ and FE $\Delta K_{eff,cl}$, were found using Eqs. (9) and (10), respectively. Accounting for the crack closure behaviour through the FE simulations for all the OP-TMF tests was done using FE $\Delta K_{eff,op}$ and FE $\Delta K_{eff,cl}$, as shown in Fig. 17(a) and (b), respectively. The collapse of the crack growth curves using the FE simulations and using the experimental data was seen to be similar, see Figs. 10 and 17. It can be observed that accounting for crack closure effects using FE σ_{cl} produces better alignment with the isothermal tests compared to the use of FE σ_{op}.

5. Discussion

For OP-TMF tests without dwell, an influence of the minimum temperature, T_{min}, on the minimum stress, σ_{min}, (see SET2-06 and SET2-05 in Fig. 7(a) and (c)) could potentially come from the fact that the

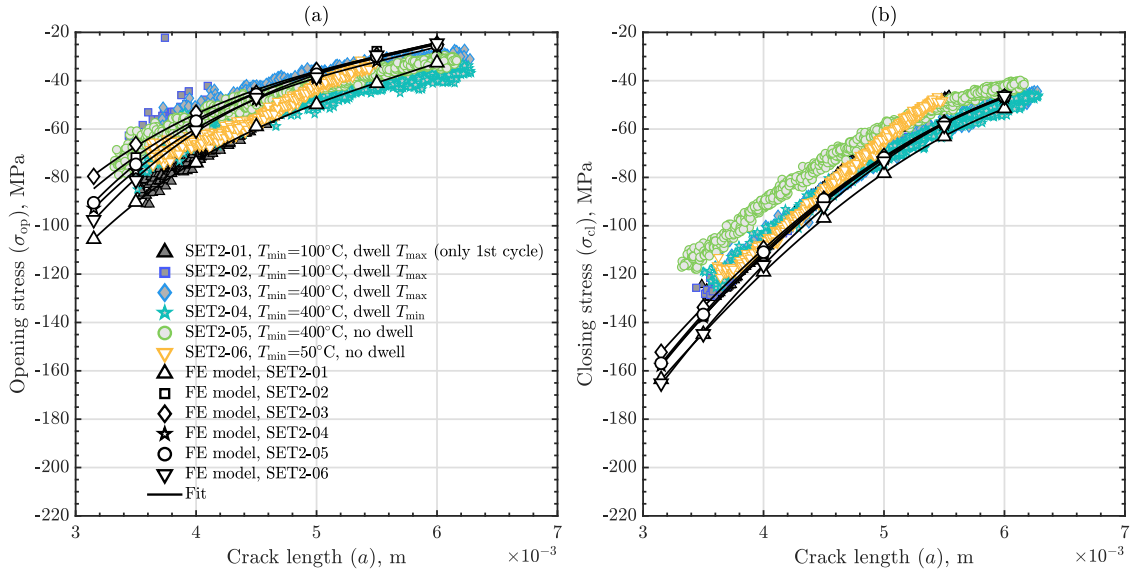

Fig. 16. Experimental and FE crack closure stresses over crack length, a, for all OP-TMF tests performed in this work, showing (a) crack opening stress, σ_{op}; (b) crack closing stress, σ_{cl}. The FE opening and closing stresses (FE σ_{op} and FE σ_{cl}) were obtained using the crack surface contact area method.

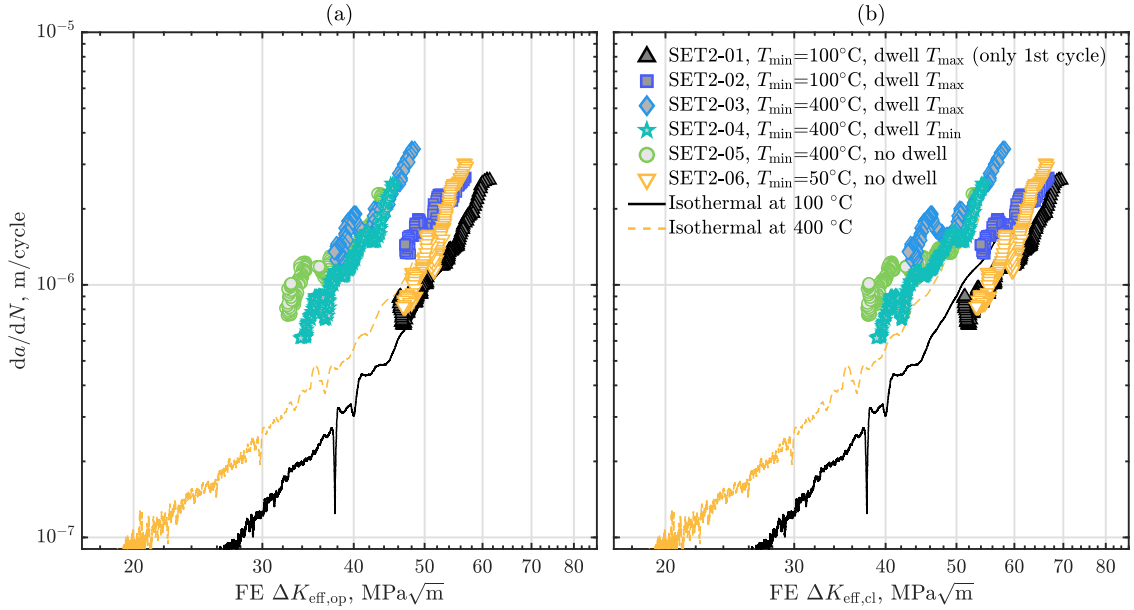

Fig. 17. Fatigue crack growth behaviour after accounting for the crack closure effects using the FE simulations of OP-TMF tests. The crack growth rate, da/dN, is plotted versus: (a) FE $\Delta K_{eff,op}$, the FE effective opening stress intensity range; (b) FE $\Delta K_{eff,cl}$, the FE effective closing stress intensity range.
Source: The isothermal test at 100 °C was taken from Azeez et al. [18].

cycle duration differs when using different T_{min}. Since the heating and cooling rates as well as the maximum temperature, T_{max}, were constant for all the OP-TMF tests, reducing T_{min} would produce longer cycles. This implies that more time is spent at high mechanical strains, ϵ_{mec}, which could cause σ_{min} to relaxes to a higher value in the 1st cycle for tests with low T_{min}, see Fig. 11. However, after the 1st cycle, the behaviour of σ_{min} was seen to be linear in the semi-log x plots in Fig. 7 and with similar slopes for all the OP-TMF tests, except for SET2-01. Meaning that the exponential relaxation behaviour of σ_{min} over the cycles, N, is identical and could be related to the creep strength at T_{max} for the material used. Adding a dwell time of 3 min at T_{max} in every cycle was seen to push σ_{min} to the same level starting from the 2nd cycle regardless of T_{min} used, see SET2-02 and SET2-03 in Fig. 7(b) and (c). This indicates that the influence of T_{min} vanishes when sufficient dwell time is introduced at T_{max} in every cycle that relaxes σ_{min} to a similar level. On the other hand, adding a dwell time of 3 min at T_{min} in every cycle instead showed no noticeable effect on σ_{min} compared to the test without dwell for the same T_{min}, see SET2-04 and SET2-05 in Fig. 7(c). For the OP-TMF test SET2-01 with a long dwell of 24 h added only in the 1st cycle, a stable level of σ_{min} over cycles was seen, see Fig. 7(a). This shows that large creep deformation at T_{max} in the 1st cycle relaxes σ_{min} to a stable level, i.e. about −200 MPa, where further cycling without any dwell at T_{max} did not cause any change to σ_{min}. Through the use of FE simulation with material parameter switching to the mid-life cyclic behaviour, an acceptable approximation of σ_{min} to the experimental results was reached, see Fig. 13. Even though some deviation of σ_{min} can be observed between the experimental and the simulated results, the difference is generally insignificant for crack length $a \geq 4$ mm as the material properties approach mid-life cyclic behaviour. The quick change in σ_{min} observed for short crack lengths,

i.e. approximately $a < 4$ mm, (see Fig. 13) is due to the exponential behaviour of σ_{min} seen over cycles (see Fig. 7). Within this region, i.e. $a < 4$ mm, a large difference in σ_{min} between the FE simulations and the experimental results is seen. However, this is only confined to the initial cycles where the material's cyclic behaviour still has not reached the stable mid-life behaviour.

A similar level of the maximum stress, σ_{max}, over the crack length, a, was observed among the OP-TMF tests with a T_{min} of 50 °C and 100 °C, see Fig. 8. However, OP-TMF tests with T_{min} of 400 °C were observed to produce a slightly lower σ_{max} compared to the other OP-TMF tests. This could be explained by the mechanical properties of the material being temperature-dependent. As the material is cooled to T_{min} during loading (see Fig. 3), lower σ_{max} is produced when using higher values of T_{min}. However, as the difference in T_{min} between 50 °C and 100 °C is relatively small, the change in the temperature-dependent mechanical properties is limited, which produce similar levels of σ_{max}. In Fig. 14, the FE simulations can be seen to produce acceptable accuracy of the σ_{max} to the experimental results. Furthermore, the addition of dwell time at T_{max} seem to have a limited influence on σ_{max}, as seen for both experimental and FE results, see Fig. 14. Also, the addition of dwell at T_{min} did not seem to affect σ_{max} as seen in the FE simulated results, see Fig. 14(c).

The crack growth behaviour was examined through the use of LEFM and the utilisation of the stress intensity factor. Although, minor inelastic deformation was observed after the 1st OP-TMF cycle (see Fig. 6(a)), it was seen to reduce with further cycling. This allowed a fair assumption of small scale yielding and acceptable crack growth rates were obtained. The OP-TMF crack growth rates showed successful collapse on the isothermal tests with temperatures similar to the minimum temperature of the OP-TMF cycle (see Fig. 10). This behaviour could indicate that the limited inelastic deformation seen in the OP-TMF tests does not play a major role and LEFM could still be applied. The crack growth behaviour observed for OP-TMF tests in Fig. 9(a) shows dependency on T_{min}, while the addition of dwell time does not seem to have an effect. In isothermal tests, the crack growth becomes faster by increasing the temperature, which is similarly observed for the OP-TMF tests when increasing T_{min}. By accounting for the crack closure behaviour using the effective opening and closing stress intensity ranges as seen in Fig. 10, all the OP-TMF tests collapsed on the isothermal tests with similar temperature as T_{min}. This indicates that the part of the OP-TMF cycle close to T_{min} largely affects the crack growth behaviour [18]. Thus, by observing Fig. 10, it would be possible to approximate the crack growth behaviour of all OP-TMF tests (with or without dwell) through the use of isothermal tests. It can also be noticed that the crack growth behaviour of OP-TMF tests is not sensitive to small changes in T_{min}, i.e. OP-TMF test with T_{min} of 50 °C and 100 °C collapsed together on the isothermal test done at 100 °C.

The crack opening and closing stresses, σ_{op} and σ_{cl}, were obtained from the experimental OP-TMF cycles using the compliance crack closure stress measurement method, which followed a global approach. On the other hand, a local approach was followed to obtain the predicted FE σ_{op} and FE σ_{cl} through the use of a crack surface contact area method. The FE crack closure stresses were seen to predict the experimental results fairly well for all crack lengths, see Fig. 16, which indicate that both the local and the global approaches were reliable.

The crack opening stress behaved similarly among all the OP-TMF tests. This behaviour is also observed for the crack closing stress among all the OP-TMF tests. This indicates that no noticeable effect is produced among OP-TMF tests with or without dwell as well as among OP-TMF tests with different T_{min}. Meaning that the crack opening and closing stresses were insensitive to the change in σ_{min} and the FE approximation was sufficient in predicting the crack closure behaviour. The crack closing stress, σ_{cl}, has been seen to be sensitive to the residual stresses introduced during the loading to σ_{max} [18]. Since σ_{max} seen in Fig. 14 do not differ dramatically among the OP-TMF tests, similar residual stresses were introduced at the crack tip during the maximum loading leading to similar levels of σ_{cl}. For the crack opening stress, σ_{op}, similar values were reached among the OP-TMF tests due to relaxation of the residual stresses at $T_{max} = 600$ °C.

Using the FE predicted crack opening and closing stresses, FE σ_{op} and FE σ_{cl}, FE effective crack opening and closing stress intensity factors, FE $\Delta K_{eff,op}$ and FE $\Delta K_{eff,cl}$, were used to collapse the crack growth curves as seen in Fig. 17. A similar collapse of the crack growth curve was observed using both the experimental and the FE predicted crack closure stresses, see Figs. 10 and 17. For both the experimental and the FE results, the use of crack closing stress, σ_{cl}, provided a better collapse of the crack growth curves compared to the use of crack opening stress, σ_{op}.

6. Conclusions

A 9–12% Cr martensitic steam turbine steel referred to as FB2 was investigated by crack propagation testing. Both isothermal and thermomechanical fatigue crack propagation tests were performed. Out-of-phase thermomechanical fatigue conditions were used to understand the crack growth behaviour for high-temperature steam turbine casing subjected to flexible operation. The inclusion of dwell and the use of three different minimum temperatures were done in the OP-TMF tests to explore their effect on the crack growth behaviour. Conclusions drawn from this study are

- An increase in the minimum temperature for OP-TMF test without dwell time produces lower minimum stress. The addition of 3 min dwell time at the maximum temperature increased the minimum stress to a similar level regardless of the minimum temperature applied, while the addition of 3 min dwell time at the minimum temperature showed no influence on the minimum stress. For the test with a long dwell time in the 1st cycle, a stable level of minimum stress is seen. The maximum stress was observed to decrease with the increase in the minimum temperature, while the addition of dwell time showed limited influence. Similar maximum stress was observed between tests with a minimum temperature of 50 °C and 100 °C.
- The crack growth behaviour of the OP-TMF tests is mainly affected by the minimum temperature while the addition of any dwell time did not produce any noticeable effects. Higher minimum temperature produced higher crack growth rates in the OP-TMF tests, which is similarly observed for isothermal tests when increasing the temperature. However, the crack growth behaviour for the OP-TMF tests was insensitive to the small change in the minimum temperature, i.e. between 50 °C and 100 °C. The crack growth curves for the OP-TMF tests were produced by utilising linear elastic fracture mechanics and the stress intensity factor.
- Crack closure was observed in all the OP-TMF tests. The crack opening stress was similar among all tests (with and without dwell and for different minimum temperatures). In addition, the crack closing stress was also similar among all the tests. Indicating that the addition of dwell and the change in minimum temperature did not influence the crack opening and closing stresses (σ_{op} and σ_{cl}).
- After compensating for the crack closure effects using the effective opening and closing stress intensity ranges ($\Delta K_{eff,op}$ and $\Delta K_{eff,cl}$), the crack growth curves collapsed on the isothermal tests with temperature similar to the minimum temperature (T_{min}) of the OP-TMF tests regardless of having a dwell or not. This indicates that part of the OP-TMF cycle close to the minimum temperature largely affects the crack growth behaviour. A better collapse of crack growth curves was observed when using the effective closing stress intensity range ($\Delta K_{eff,cl}$) compared to the use of the effective opening stress intensity range ($\Delta K_{eff,op}$).

- The use of a three-dimensional FE model with a sharp stationary crack and material parameters switching from initial to mid-life cyclic behaviour achieved acceptable accuracy in predicting the experimental hysteresis curves of the OP-TMF tests. The FE prediction of the crack closure stresses, using the crack surface contact area method, was able to predict the experimental crack closure stresses obtained using the compliance crack closure measurement method.
- Accounting for crack closure effects using the experimental and the FE predicted crack closure stresses produced a similar collapse of the crack growth curves on the isothermal tests. The use of FE simulations was successful in predicting the effective opening and closing stress intensity ranges. In addition, the collapse of the crack growth curves on the isothermal tests present the possibility of approximating the OP-TMF crack growth behaviour through isothermal tests.

Declaration of competing interest

The authors declare that they have no known competing financial interests or personal relationships that could have appeared to influence the work reported in this paper.

Acknowledgement

SIEMENS AG is acknowledged for their support and providing the material used for testing.

References

[1] Topel M, Guédez R, Laumert B. Impact of increasing steam turbine flexibility on the annual performance of a direct steam generation tower power plant. Energy Procedia 2015;69:1171–80, Int. Conf. on Concentrating Solar Power and Chemical Energy Systems, SolarPACES 2014.
[2] Impram S, Varbak Nese S, Oral B. Challenges of renewable energy penetration on power system flexibility: A survey. Energy Strategy Rev 2020;31:100539.
[3] Tomala M, Rusin A, Wojaczek A. Risk-based planning of diagnostic testing of turbines operating with increased flexibility. Energies 2020;13.
[4] Lifetime assessment of steam turbine casing, Volume 8: Microturbines, turbochargers and small turbomachines; Steam turbines of turbo expo: Power for land, sea, and air. 2015, http://dx.doi.org/10.1115/GT2015-43495, v008T26A032.
[5] Choi W, Hyun J. A life assessment for steam turbine casing using inelastic analysis. Modern Phys Lett B 2008;22:1141–6.
[6] Bhanu Sankara Rao K, Raj B, Nagesha A. Fatigue testing: Thermal and thermo-mechanical. In: Reference module in materials science and materials engineering. Elsevier; 2017, http://dx.doi.org/10.1016/B978-0-12-803581-8.03464-0.
[7] ASTM E2368-10. Standard practice for strain controlled thermomechanical fatigue testing. Standard, West Conshohocken, PA: ASTM International; 2017, http://dx.doi.org/10.1520/E2368-10R17.
[8] Jacobsson L, Persson C, Melin S. Thermo-mechanical fatigue crack propagation experiments in inconel 718. Int J Fatigue 2009;31:1318–26.
[9] Palmer J, Jones J, Dyer A, Smith R, Lancaster R, Whittaker M. Development of test facilities for thermo-mechanical fatigue testing. Int J Fatigue 2019;121:208–18.
[10] Jacques S, Lynch M, Wisbey A, Stekovic S, Williams S. Development of fatigue crack growth testing under thermo-mechanical fatigue conditions. Mater High Temp 2013;30:49–61.
[11] Stekovic S, Jones J, Engel B, Whittaker M, Norman V, Rouse J, Pattison S, Hyde C, Härnman P, Lancaster R, Leidermark D, Moverare J. Devtmf – towards code of practice for thermo-mechanical fatigue crack growth. Int J Fatigue 2020;138:105675.
[12] Pretty CJ, Whitaker MT, Williams SJ. Thermo-mechanical fatigue crack growth of rr1000. Materials 2017;10.
[13] Ewest D, Almroth P, Sjödin B, Leidermark D, Simonsson K. Isothermal and thermomechanical fatigue crack propagation in both virgin and thermally aged haynes 230. Int J Fatigue 2019;120:96–106.
[14] Almroth P, Gustafsson D, Loureiro Homs J, Simonsson K. Out-of-phase thermo-mechanical fatigue crack growth and the effect of the compressive minimum load level on crack closure at notches. Int J Fatigue 2020;141:105906.
[15] Loureiro-Homs J, Almroth P, Palmert F, Gustafsson D, Simonsson K, Eriksson R, Leidermark D. Accounting for crack closure effects in tmf crack growth tests with extended hold times in gas turbine blade alloys. Int J Fatigue 2021;142:105917.
[16] Wolf E. Fatigue crack closure under cyclic tension. Eng Fract Mech 1970;2:37–45.
[17] Dai J, Marchand NJ, Hongoh M. Thermal mechanical fatigue crack growth in titanium alloys: Experiments and modelling. West Conshohocken, PA: ASTM International; 1996, p. 187–209. http://dx.doi.org/10.1520/STP16454S.
[18] Azeez A, Norman V, Eriksson R, Leidermark D, Moverare J. Out-of-phase thermomechanical fatigue crack propagation in a steam turbine steel — modelling of crack closure. Int J Fatigue 2021;149:106251.
[19] Wärner H, Calmunger M, Chai G, Johansson S, Moverare J. Thermomechanical fatigue behaviour of aged heat resistant austenitic alloys. Int J Fatigue 2019;127:509–21.
[20] Fischer T, Kuhn B. Frequency and hold time influence on crack growth behavior of a 9%–12% cr ferritic martensitic steel at temperatures from 300 °C to 600 °C in air. Int J Fatigue 2018;112:165–72.
[21] Makhlouf K, Jones J. Effects of temperature and frequency on fatigue crack growth in 18% cr ferritic stainless steel. Int J Fatigue 1993;15:163–71.
[22] Lim BS, Jeong CS, Keum YT. Effect of temperature on fatigue crack growth in p92 steel. Met Mater Int 2003;9:543–7.
[23] Palmert F, Moverare J, Gustafsson D. Thermomechanical fatigue crack growth in a single crystal nickel base superalloy. Int J Fatigue 2019;122:184–98.
[24] Gustafsson D, Moverare J, Johansson S, Hörnqvist M, Simonsson K, Sjöström S, Sharifimajda B. Fatigue crack growth behaviour of inconel 718 with high temperature hold times. Procedia Eng 2010;2:1095–104, Fatigue 2010.
[25] Hong H, Kang J, Choi B, Kim I, Yoo Y, Jo C. A comparative study on thermomechanical and low cycle fatigue failures of a single crystal nickel-based superalloy. Int J Fatigue 2011;33:1592–9.
[26] Deng W, Xu J, Hu Y, Huang Z, Jiang L. Isothermal and thermomechanical fatigue behavior of inconel 718 superalloy. Mater Sci Eng A 2019;742:813–9.
[27] Pan X-M, Li X, Chang L, Zhang G-D, Xue F, Zhao Y-F, Zhou C-Y. Thermal-mechanical fatigue behavior and lifetime prediction of p92 steel with different phase angles. Int J Fatigue 2018;109:126–36.
[28] Barrett RA, Hyde CJ, O'Donoghue PE, Leen SB. Thermomechanical fatigue in 9-12cr steels: Life prediction models and the effect of tensile dwell periods. Int J Fatigue 2019;126:335–45.
[29] Zhao P, Xuan F-Z, Wu D-L. Cyclic softening behaviors of modified 9–12% cr steel under different loading modes: Role of loading levels. Int J Mech Sci 2017;131–132:278–85.
[30] Führer U, Aktaa J. Modeling the cyclic softening and lifetime of ferritic-martensitic steels under creep-fatigue loading. Int J Mech Sci 2018;136:460–74.
[31] Mishnev R, Dudova N, Kaibyshev R. Effect of microstructural evolution on the cyclic softening of a 10% cr martensitic steel under low cycle fatigue at 600 °C. Int J Fatigue 2020;134:105522.
[32] Illg W, Mcevily AJ. The rate of fatigue-crack propagation for two aluminum alloys under completely reversed loading. NASA Technical Note D-52, Langley Field, Va: Langley Research Center; 1959, URL: https://hdl.handle.net/2027/uiug.30112106741124.
[33] McClung R, Sehitoglu H. On the finite element analysis of fatigue crack closure—2. numerical results. Eng Fract Mech 1989;33:253–72.
[34] Toribio J, Matos J-C, González B. Numerical modeling of plasticity-induced fatigue crack growth retardation due to deflection in the near-tip area. Metals 2021;11.
[35] Masuda K, Ishihara S, Oguma N. Effect of specimen thickness and stress intensity factor range on plasticity-induced fatigue crack closure in a7075-t6 alloy. Materials 2021;14.
[36] Fischer C, Schweizer C, Seifert T. A crack opening stress equation for in-phase and out-of-phase thermomechanical fatigue loading. Int J Fatigue 2016;88:178–84.
[37] Patriarca L, Foletti S, Beretta S. A comparison of dic-based techniques to measure crack closure in lcf. Theor Appl Fract Mech 2018;98:230–43.
[38] Loureiro-Homs J, Gustafsson D, Almroth P, Simonsson K, Eriksson R, Leidermark D. Accounting for initial plastic deformation for fatigue crack growth predictions under tmf loading condition. Int J Fatigue 2020;136:105569.
[39] Azeez A, Eriksson R, Leidermark D, Calmunger M. Low cycle fatigue life modelling using finite element strain range partitioning for a steam turbine rotor steel. Theor Appl Fract Mech 2020;107:102510.
[40] Di Gianfrancesco A, Blum R. 24 - A-usc programs in the european union. In: Gianfrancesco A Di, editor. Materials for ultra-supercritical and advanced ultra-supercritical power plants. Woodhead Publishing; 2017, p. 773–846. http://dx.doi.org/10.1016/B978-0-08-100552-1.00024-5.
[41] Kern T-U, Staubli M, Scarlin B. The European efforts in material development for 650 °C USC power plants - COST 522. ISIJ Int 2002;42:1515–9.
[42] Kern TU, Mayer KH, Donth B, Zeiler G, Di Gianfrancesco A. The european efforts in development of new high temperature rotor materials - cost536. In: Proc. of 9th Liege conf. on materials for advanced power engineering. Liege, Belgium; 2010, pp. 27–36.
[43] Abe F. 10 - New martensitic steels. In: Gianfrancesco A Di, editor. Materials for ultra-supercritical and advanced ultra-supercritical power plants. Woodhead Publishing; 2017, p. 323–74. http://dx.doi.org/10.1016/B978-0-08-100552-1.00010-5.

[44] Kaybyshev R, Skorobogatykh V, Shchenkova I. New martensitic steels for fossil power plant: Creep resistance. Phys Met Metallogr 2010;109:186–200.
[45] Holdsworth S. Creep resistant materials for steam turbines. In: Reference module in materials science and materials engineering. Elsevier; 2016, http://dx.doi.org/10.1016/B978-0-12-803581-8.02063-4.
[46] Zeiler G. 6 - martensitic steels for rotors in ultra-supercritical power plants. In: Gianfrancesco A Di, editor. Materials for ultra-supercritical and advanced ultra-supercritical power plants. Woodhead Publishing; 2017, p. 143–74. http://dx.doi.org/10.1016/B978-0-08-100552-1.00006-3.
[47] Holdsworth SR. Creep-fatigue properties of high temperature turbine steels. Mater High Temp 2001;18:261–5.
[48] Mishnev R, Dudova N, Kaibyshev R. On the origin of the superior long-term creep resistance of a 10% cr steel. Mater Sci Eng A 2018;713:161–73.
[49] ASTM E1457-07. Standard test method for measurement of creep crack growth times in metals. Standard, West Conshohocken, PA: ASTM International; 2007, http://dx.doi.org/10.1520/E1457-07.
[50] ISO 12108:2002(E). Metallic materials — Fatigue testing — Fatigue crack growth method. Standard, Geneva, CH: International Organization for Standardization; 2002.
[51] Paris P, Erdogan F. A critical analysis of crack propagation laws. J Basic Eng 1963;85:528–33.
[52] ASTM E647-13a. Standard test method for measurement of fatigue crack growth rates. Standard, West Conshohocken, PA: ASTM International; 2013, http://dx.doi.org/10.1520/E0647-13A.
[53] ABAQUS user's manual, version 2017. Johnston, RI, USA: Dassault Systemes; 2017.
[54] Hosford WF. Mechanical behavior of materials. 2nd ed.. Cambridge University Press; 2009, http://dx.doi.org/10.1017/CBO9780511810923.
[55] Eriksson R, Moverare J, Chen Z. A low cycle fatigue life model for a shot peened gas turbine disc alloy. Int J Fatigue 2019;124:34–41.
[56] Leidermark D, Simonsson K. Procedures for handling computationally heavy cyclic load cases with application to a disc alloy material. Mater High Temp 2019;36:447–58.